NASA Technical Memorandum 88792

NASA-TM-88792 19860019799

Experimental Classical Flutter Results of a Composite Advanced Turboprop Model

O. Mehmed and K.R.V. Kaza
Lewis Research Center
Cleveland, Ohio

July 1986

NASA

ENTER:

DISPLAY 42/6/1
86N29271*# ISSUE 20 PAGE 3182 CATEGORY 39 RPT#: NASA-TM-88792
E-3127 NAS 1.15:88792 86/07/00 18 PAGES UNCLASSIFIED DOCUMENT
UTTL: Experimental classical flutter reesults of a composite advanced turboprop model
AUTH: A/MEHMED, O.; B/KAZA, K. R. V.
CORP: National Aeronautics and Space Administration. Lewis Research Center, Cleveland, Ohio.
SAP: Avail: NTIS HC A02/MF A01
CIO: UNITED STATES Presented at the Bisplinghoff Memorial Symposium on Recent Trends in Aeroelasticity, Structures and Structural Dynamics, Gainesville, Fla., 6-7 Feb., 1986; sponsored by Fla. Univ.
MAJS: /*FLUTTER ANALYSIS/*MODELS/*PROP-FAN TECHNOLOGY/*PROPELLER BLADES/* TURBOPROP ENGINES
MINS: / AERODYNAMIC COEFFICIENTS/ ANGLE OF ATTACK/ CASCADE FLOW/ COUPLING/ PITCH (INCLINATION)
ABA: Author

EXPERIMENTAL CLASSICAL FLUTTER RESULTS OF A COMPOSITE ADVANCED TURBOPROP MODEL*

O. Mehmed and K.R.V. Kaza
National Aeronautics and Space Administration
Lewis Research Center
Cleveland, Ohio 44135

SUMMARY

Experimental results are presented that show the effects of blade pitch angle and number of blades on classical flutter of a composite advanced turboprop (propfan) model. An increase in the number of blades on the rotor or the blade pitch angle is destablizing which shows an aerodynamic coupling or cascade effect between blades. The flutter came in suddenly and all blades vibrated at the same frequency but at different amplitudes and with a common predominant phase angle between consecutive blades. This further indicates aerodynamic coupling between blades. The flutter frequency was between the first two blade normal modes, signifying an aerodynamic coupling between the normal modes. Flutter was observed at all blade pitch angles from small to large angles-of-attack of the blades. A strong blade response occurred, for four blades at the two-per-revolution (2P) frequency, when the rotor speed was near the crossing of the flutter mode frequency and the 2P order line. This is because the damping is low near the flutter condition and the interblade phase angle of the flutter mode and the 2P response are the same.

E-3127

INTRODUCTION

The unconventional features of the propfan add complexity to its aeroelastic analysis. The blades are thin and flexible, thus deflections due to centrifugal and aerodynamic loads are large. Hence, analyses require geometric nonlinear theory of elasticity. Also, the blades are of low aspect ratio and large sweep, and operate in subsonic, transonic, and possibly supersonic flows. Therefore, three-dimensional, unsteady aerodynamic theory is required for accurate analysis. The blades have large sweep and twist, which couples blade bending and torsion motions, and are plate-like structures because of their low aspect ratio. These factors require a finite element structural model for accurate analysis. Then, there are six or more blades on the rotor

---

*Material presented at the Bisplinghoff Memorial Symposium on Recent Trends in Aeroelasticity, Structures, and Structural Dynamics sponsored by the University of Florida, Gainesville, Florida, February 6-7, 1986.

which means aerodynamic coupling between blades or cascade effects should be considered. These features require the use of both experimental and analytical work to understand propfan aeroelastic phenomena and to develop aeroelastic analysis methods for the design of propfans.

Classical flutter of a propfan occurred unexpectedly during an earlier wind tunnel experiment on a model with ten highly swept titanium blades. For that model, the blade tip relative flow at flutter was transonic, between Mach 0.95 and 1.05, and the flutter frequency was almost equal to the blade first normal mode frequency. Also, based on the three-quarter radius and the semichord, the reduced flutter frequency was between 0.17 and 0.19 and the blade-to-air mass ratio was 115. The measured flutter speed was much lower than predicted by two-dimensional, subsonic, unsteady, isolated airfoil aerodynamic theory with a beam structural model for the blade. The difference between theory and experiment prompted an experimental and analytical effort. To evaluate the effect of aerodynamic coupling on flutter, two-, five-, and ten-blade configurations of the highly swept model were tested. These experiments revealed that aerodynamic coupling significantly lowered the flutter boundaries, and that the flutter was classical with coupling between the normal modes of the blade. The test results provided guidance to refine analytical models. The first phase of refinements included incorporation of two-dimensional, subsonic, unsteady, cascade aerodynamics with a sweep correction, based on similarity laws, and an idealized beam structural model of each blade. Analytical and experimental results from that study were correlated in reference [1]. The second phase of analytical refinements included the use of mode shapes and frequencies from a finite-element plate structural model in a modal flutter analysis with the same aerodynamics as in reference [1]. References [2] and [3] document some of this analytical work and correlate analytical and experimental results. The correlation between theory and experiment in references [1,2 and 3] varied from poor to good. Hence, there was a need to further understand the phenomena and to get data in the subsonic flow regime in order to develop and validate analytical models.

The present study was then planned to obtain flutter data in subsonic relative flows at the blade tip and to further investigate the phenomena of propfan unstalled bending-torsion flutter. A blade design was tailored by the use of composite material. This paper describes the model blades, the experiment and the results.

FLUTTER MODEL BLADES

A flutter model, designated SR3C-X2, made from graphite-ply/epoxy-matrix material was designed with the flutter analysis described in reference [2]. The blade was designed for research purposes only and was not dynamically scaled from a large blade. Under a cooperative effort, NASA Lewis Research Center developed the finite element model and provided the modal data for the flutter analysis, Hamilton Standard performed the flutter analysis and NASA Ames fabricated the blades.

The design was tailored by the orientation of the unidirectional tape material used for blade construction. Figure 1 shows the ply directions. The blades had 80 percent of their plys oriented along the 0° axis shown. The remaining plys were oriented along the ±22.5° directions.

Figure 2 shows a photo of the blade. It has a geometric midchord sweep of 45° at its tip and a nominal tip diameter of 0.62 m (2 ft). The blade-to-air mass ratio is 33.

Figure 3 shows the variation with rotational speed of natural frequencies, in vacuum, for the SR3C-X2 blade from an MSC NASTRAN finite element plate model. The measured average bench natural frequency of eight blades is also indicated for comparison. Figure 4 shows hologram photos of the measured bench mode shapes and corresponding natural frequencies of one of the blades. Here, the black fringes represent constant displacement contours and the whitest fringes are nodes or areas of near zero displacement. It can be seen from the displacement contours that the first mode is primarily flexural but also has a large degree of torsion and the second mode is primarily torsional near the tip. It will be shown later that flutter occurred between these two modes.

FLUTTER EXPERIMENT

The experiment was conducted in the Lewis 8-by-6-ft (2.44-by-1.83 m) wind tunnel at tunnel Mach numbers from 0.36 to 0.75 and rotor speeds up to 8000 rpm. Eight- and four-blade rotors were tested to investigate the degree of aerodynamic coupling between blades. The blades were mounted in a hub which can be considered rigid. Figure 5 shows the rotors in the wind tunnel. The rotor was driven by an air turbine and its axis was aligned with the tunnel flow.

Blade mounted strain gages provided the vibration data. Each blade had at least one gage, since the blade amplitudes at flutter were expected to differ. Figure 6 shows the instrumentation installed for the two rotors. The number of strain gages was limited since only ten signals could be taken from the rotor. The gages were located at the points of maximum strain for the first four normal blade modes, as determined by finite element analysis. Only dynamic strain signals were recorded and monitored during the test. Gage 2 usually had the maximum response at flutter for both rotors but Gage 3 gave a greater response when the flutter mode changed with the eight blade rotor. The flutter modes are discussed later.

The test variables were tunnel Mach number, rotor speed and propeller blade pitch. The blade pitch angle, $\beta_{0.75R}$ - the acute angle that the blade chord makes with the plane of rotation at the 0.75 blade radius, was locked manually. The wind tunnel was then started and a Mach number was set. The propeller was left in the unpowered or windmilling condition during tunnel speed changes. The rotor was then powered and its speed slowly increased until flutter occurred or an operating limit was reached.

Flutter was not always reached because of three operating limits. At some conditions the rpm was limited by the power available from the rotor air drive system. Then, rotor speed was limited to 8000 rpm because of blade strength. Also, because of blade strength there was an intended limit of 700 microstrain (0-peak) on blade dynamic strain - it was exceeded at times during flutter. To get out of high stress conditions during flutter the following was done: in the powered rotor conditions, the rotor speed was dropped; in the unpowered rotor condition, the tunnel Mach number was dropped.

EXPERIMENTAL RESULTS

Figure 7 summarizes the operating boundaries of the experiment. The range of test variables are: tunnel Mach number, 0.36 to 0.75; rotor speed, windmill rpm to 8000 rpm; and blade pitch angle, 56.6° to 68.4°. The operating procedure described above traces a vertical path on the figure from the windmilling rpm to the boundary. Two types of blade activity are identified. Points labeled "F" designated blade flutter. Points labeled "2P" designate a blade forced response at a two-per-revolution frequency. The rig power limit existed at points labeled "P" and the blade rpm limit at points labeled "R". Open symbols represent the four-blade rotor and closed symbols the eight-blade rotor.

Comparing the flutter boundaries (points labeled "F") for the two rotors at the same blade angle and Mach number, it is seen that the critical rpm is higher for four than for eight blades at all conditions. This indicates that aerodynamic coupling (the cascade effect) reduces the flutter speed. The flutter occurred at small angles-of-attack of the blades (windmilling points), as well as large angles-of-attack at all blade pitch angles.

The flutter came in with explosive suddenness. The amplitude would grow from very low to very high levels with an increase in rpm of about 1 percent. Figure 8(a) and (b) illustrate the rapid increase in stress amplitude, at two different conditions. Figure 8(a) is for a tip torsion gage and figure 8(b) is for a flexure sensitive gage. In one case, the strain amplitude reached about three times its intended limit, and in the other over four times. Most of the flutter points in figure 7 are shown at the rotational speed where the sudden stress rise occurred. In some cases the authors became cautious and used the unsteadiness of the flutter frequency amplitude peak, from an on-line spectral analyzer, to infer the proximity to the explosive growth point. Nevertheless, it is estimated that all flutter points in figure 7 are within 80 rpm of the explosive condition. The arrows of figure 8 indicate the direction of rpm change.

Time history records at the flutter condition show a limit amplitude was reached at the large displacements experienced. A limit amplitude is possible due to aerodynamic and/or structural nonlinearities which occur at large displacement amplitudes. Nonlinear response was also evidenced by the presence of harmonics of the flutter frequency in the spectra at these conditions. Although high stresses were reached no blades were damaged during the test.

Figure 9 shows the stress amplitudes during flutter at typical conditions. The blade amplitudes varied because the individual blade properties differed, that is, the rotor was mistuned.

Figure 10 shows the flutter data of figure 7 replotted to display the effect of blade pitch angle on the flutter boundaries. The flutter boundaries for eight and four blades are shown on separate plots. Note, a blade tip rotational Mach number ordinate scale is included, based on an airflow static temperature of 529° R. It can be seen that an increase an blade pitch angle decreases the critical rotational speed at a constant tunnel Mach number for all cases, except for four blades at windmill conditions (marked "W"). This decrease is due to a change in aerodynamic coupling between blades, a change in the blade loading and/or a change of the blades normal mode shapes and frequencies under centrifugal loading.

For a rotor of N identical blades at flutter, the phase angle between adjacent blades is the same. Thus, in a rotating frame of reference, a traveling wave can describe the flutter. A forward traveling wave is defined as one traveling in the direction of rotation. The phase angle between blades (interblade phase angle), in degrees, for each of the possible flutter modes is given by

$$\sigma_k = \frac{360\ k}{N} \quad ; \quad k = 0,1,2,\ldots,N-1 \qquad (1)$$

where k is the phase angle index.

Figure 11(a) is a plot of the measured phase angle at flutter of each blade relative to blade 1 for the four-blade rotor. The possible interblade phase angle modes, given by equation 1, are represented by the lines thru the origin. The x-axis represents the 0° phase angle. The figure shows that the predominant phase angle is 180°. This corresponds to a 2 nodal diameter pattern (the number of diametral node lines around the rotor). Some data points fall off the 180° mode line, hence, the actual phase angle between blades varied around the rotor. This is because the rotor was mistuned, and more than one interblade phase angle mode participated simultaneously.

Similarly, figure 11(b) is a plot of the measured phase angle of each blade relative to blade 1 at flutter for the eight-blade rotor. Again, the interblade phase angle mode lines are shown. The eight blade data also shows evidence of mistuning. In addition, it displays a change of the predominant flutter mode with blade pitch. At a blade pitch of 61.6° the 225° mode is predominant, which is the same as -135°, and corresponds to a backward traveling wave of 3 nodal diameters. Then, at a blade pitch of 68.4° the 180° mode, 4 nodal diameter pattern, is predominant. Furthermore, at 56.6° blade pitch both the 180° and the 225° modes are evident.

Figures 12(a) and (b) give the measured flutter frequencies for the four-blade and the eight-blade rotors respectively. The harmonic order excitation lines of rotational speed and the analytically predicted first and second natural mode lines are also shown. For both

rotor configurations the flutter mode frequency falls between 254 and 284 Hz and is between the first two normal modes indicating aerodynamic coupling of the normal modes. In contrast, the flutter frequency for the rotor of titanium blades described in reference [1] was very close to the first blade normal mode frequency. This indicates a weaker aerodynamic coupling between normal modes for the titanium blades. The difference is caused by the lower blade-to-air mass ratio for the composite blades. Note, the flutter frequencies are nearly the same for four and eight blades, showing only a small effect of cascade aerodynamics on the flutter frequencies.

A significant blade response occurred with the four-blade rotor at the 2P frequency. Referring to figure 12(a), this occurred when the flutter mode was near the crossing with the 2P order excitation line. The points labeled "2P" on figure 7 designate these respondse points. This response occurs because the damping is low near the flutter condition and the interblade phase angle of the flutter mode and the 2P response are the same for four blades. Of course, a source of excitation at the 2P frequency is implied. This excitation source is not understood at this time. No corresponding blade response occurred with the eight-blade rotor. This is because the flutter frequency did not approach as near to the 2P excitation line (see figure 12(b)) and the interblade phase angle of the flutter mode and a 2P response is different for eight blades.

Figure 13(a) shows a spectrum of the strain amplitude near the 2P/flutter mode speed crossing of the four-blade rotor. The 1P (127 Hz) and 2P (254 Hz) frequencies are labeled, as well as frequencies at 264 and 274 Hz respectively ("F"). The strongest response is at the (2P) 254 Hz frequency but there is also a weaker response at 274 Hz which is the flutter mode frequency. In addition, there is a lower amplitude peak labeled 264 Hz. It is possible to have more than one interblade phase angle mode close to instability at the same time. The 264 Hz frequency is inferred to be such a dual flutter mode. Typically, a second frequency peak, of lower amplitude, was observed in the data near the flutter frequency.

Figure 13(b) shows a strain amplitude spectrum of the four-blade rotor, at 5160 rpm, away from the 2P crossing. Here, a large amplitude exists only at the 264 Hz flutter frequency. There was no evidence of a 3P response with either four or eight blades, although the flutter mode crosses the 3P order line. This indicates that a source of 3P excitation was not present.

Figure 14 shows the reduced flutter frequency, k_f, plotted against relative Mach number for both rotors. The reduced flutter frequency is based on semichord and the relative Mach number are calculated at the blade 0.75 radius. The data shows a decrease of reduced flutter frequency with an increase of relative Mach number. The only exception is with four blades at the windmill points, labeled "W". The reduced flutter frequency falls between 0.34 and 0.41 for eight blades, and 0.31 and 0.38 for four blades.

Figure 15 shows the blade tip relative Mach number at flutter plotted against rotational speed for both rotors. The data indicate

that the flow is in the high subsonic regime. The trend of the data for eight blades at each of the three blade angles shows a rise and then a fall of blade tip relative Mach number as rotor speed is increased. Whereas, the data for four blades is more random and shows no such trend. The blade tip relative Mach number at flutter falls between 0.77 and 0.87 for eight blades and 0.80 and 0.90 for four blades. In general, flutter occurred at lower relative Mach numbers for eight than four blades at the same blade angle.

OBSERVATIONS AND CONCLUSION

An experimental study was performed with a propfan model to obtain flutter data in subsonic relative flows at the blade tip and to investigate the phenomena of propfan unstalled bending-torsion flutter. Composite material was used to tailor the blade structural properties to obtain flutter in subsonic relative flows at the blade tip. Based on the results of this study the following observations and conclusions are made:

1. Classical bending-torsion unstalled flutter was observed. The flutter frequency was between the first two normal modes, indicating an aerodynamic coupling effect between the normal modes, and the flutter occurred from small to large angles-of-attack of the blades.

2. With eight blades flutter occurred predominantely in either the 180° (four nodal diameter) or 225° (three nodal diameter, backward) rotor flutter mode, whereas, with four blades flutter occurred predominantely in the 180° (two nodal diameter) rotor flutter mode. This indicates an aerodynamic coupling (cascade effect) between the blades and that the interblade phase angle mode at flutter is affected by the blade pitch angle.

3. The flutter frequencies were identical on all the blades but the strain amplitudes were not. The strain amplitude variation is attributed to blade frequency mistuning. This also shows an aerodynamic coupling effect between the blades.

4. Increasing the number of blades on the rotor is destablizing. This is inferred to be due to a difference in the aerodynamic coupling between blades.

5. Increasing the blade pitch angle is destablizing. This may be due to a change in aerodynamic coupling between blades, a change in the blade loading and/or a change of the blade normal mode shapes and frequencies under centrifugal loading.

6. The reduced flutter frequency was between 0.34 and 0.41 for eight blades and between 0.31 and 0.38 for four blades.

7. The blade tip relative Mach number at flutter was between 0.77 and 0.87 for eight blades and between 0.80 and 0.90 for four blades.

8. A strong blade response occurred with four blades at the two-per-revolution frequency when the rotational speed was near the crossing of the flutter mode frequency and the 2P order line. This is because the damping is low near the flutter condition and the interblade phase angle of the flutter mode and the 2P response are the same.

REFERENCES

1. Mehmed, O., et al.: Bending-Torsion Flutter of a Highly Swept Advanced Turboprop. NASA TM-82975, 1982.

2. Elchuri, V., and Smith, G.C.C.: Flutter Analysis of Advanced Turbopropellers. 24th Structures, Structural Dynamics and Materials Conference; Part 2, AIAA, 1983, pp. 160-165.

3. Turnberg, J.E.: Classical Flutter Stability of Swept Propellers. AIAA Paper 83-0847-CP; May 1983.

PLY DIRECTION	PERCENT TOTAL PLYS
0^0	80
$\pm 22.5^0$	20

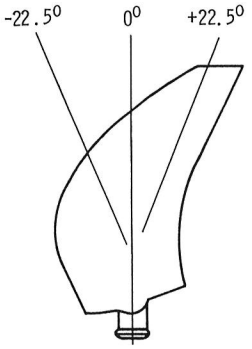

Figure 1. - Ply directions for flutter blade.

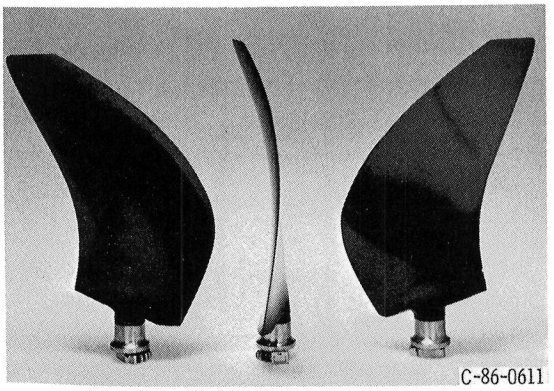

Figure 2. - SR3C - X2 flutter model blade.

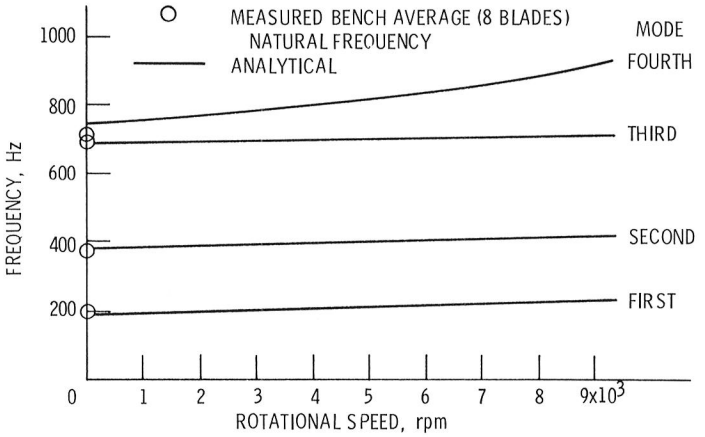

Figure 3. - Variation of natural frequency with rotational speed, $\beta_{0.75R} = 57^0$, SR3C-X2 model blades.

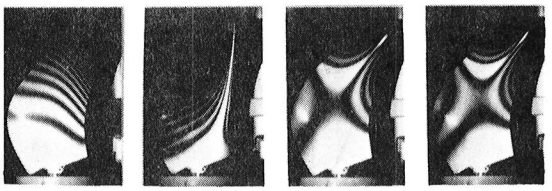

C-86-3955

Figure 4. - Bench measured natural frequencies and mode shapes, SR3C - X2 model, blade number 6.

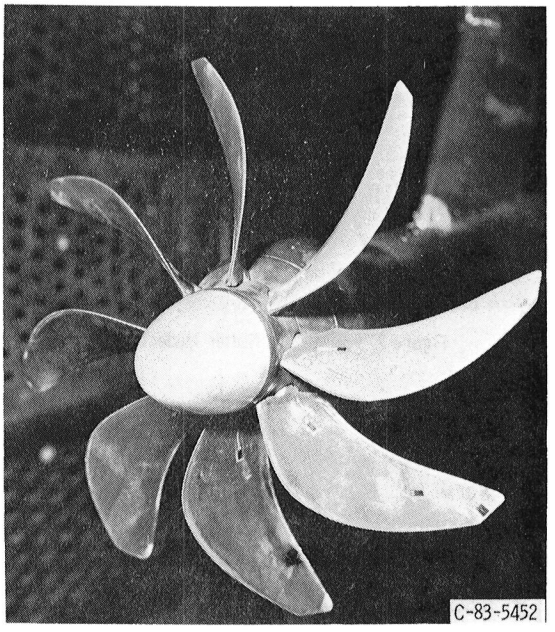

(a) 8 - blade rotor.

Figure 5. - SR3C - X2 model installation in the Lewis 8x6 ft wind tunnel.

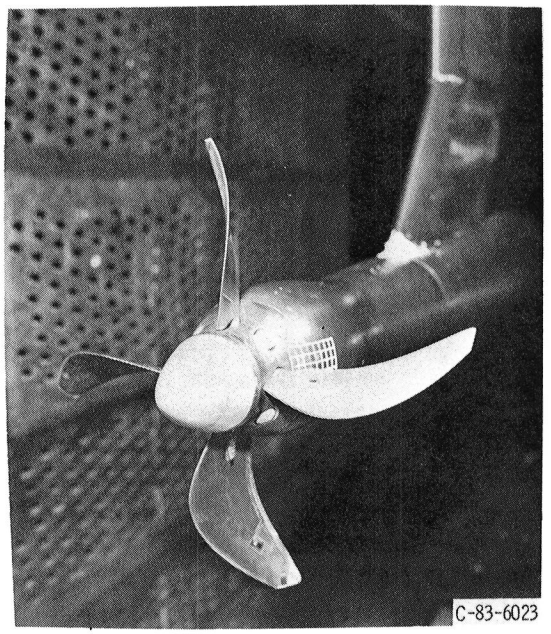

(b) 4-blade rotor.

Figure 5. - Concluded.

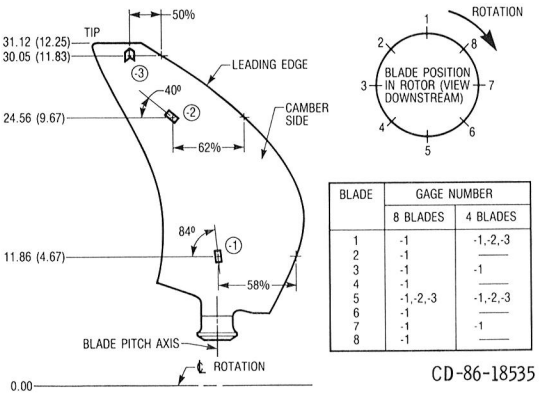

BLADE	GAGE NUMBER	
	8 BLADES	4 BLADES
1	-1	-1,-2,-3
2	-1	——
3	-1	-1
4	-1	——
5	-1,-2,-3	-1,-2,-3
6	-1	——
7	-1	-1
8	-1	——

CD-86-18535

Figure 6. - Blade strain gage installation, SR3C-X2 model.

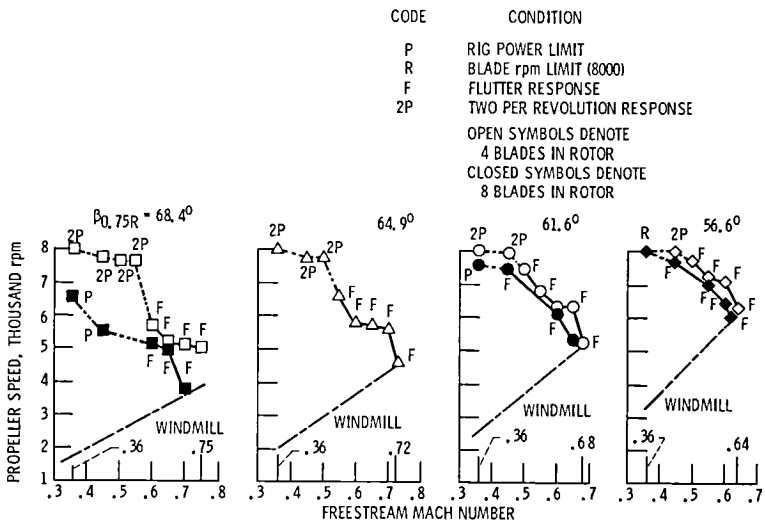

Figure 7. - Operating boundaries of the SR3C-X2 flutter experiment, 8x6-ft wind tunnel.

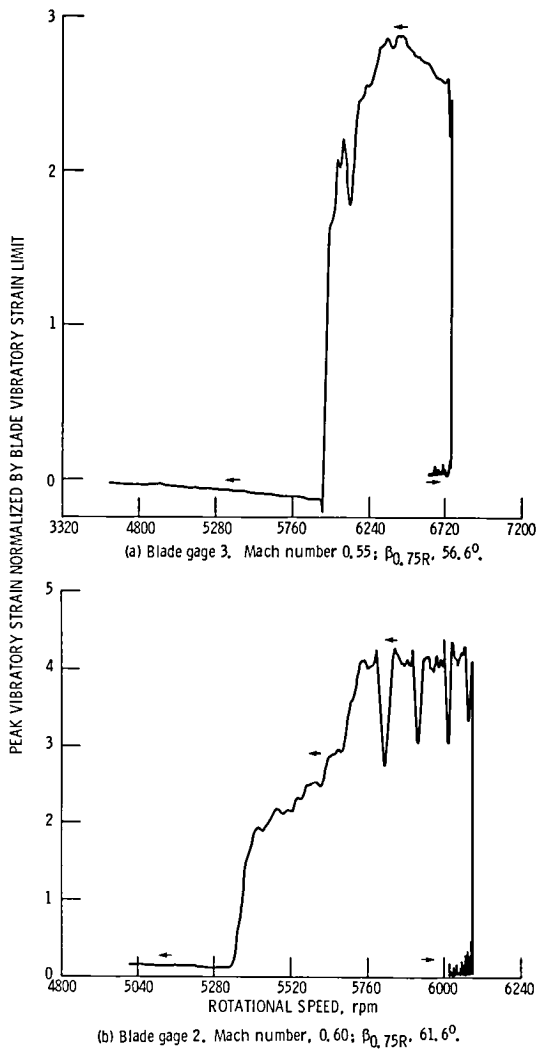

(a) Blade gage 3. Mach number 0.55; $\beta_{0.75R}$, 56.6°.

(b) Blade gage 2. Mach number, 0.60; $\beta_{0.75R}$, 61.6°.

Figure 8. - Peak strain amplitude variation with rpm at flutter, 8-blade rotor, SR3C-X2 model.

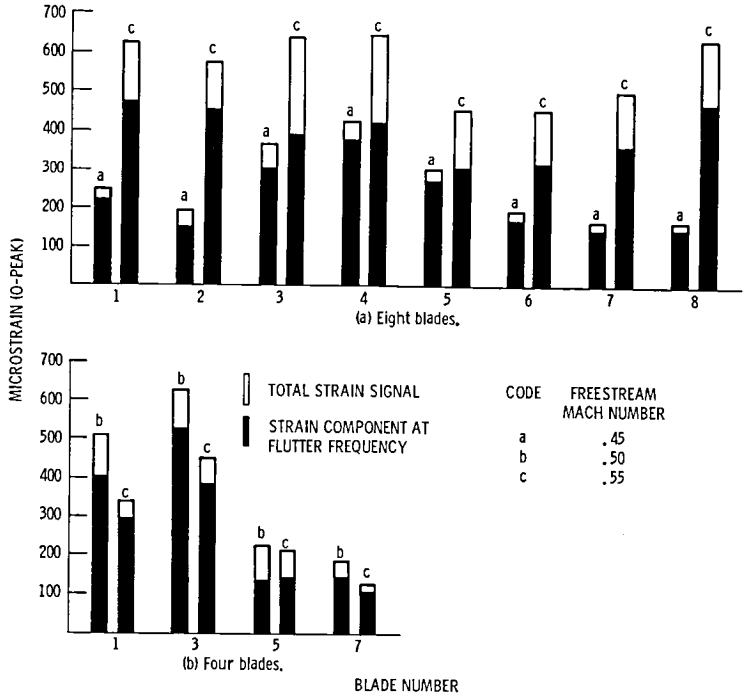

Figure 9. - Typical blade-to-blade variation in strain amplitudes at flutter, $\beta_{0.75R} = 56.6^{\circ}$, blade gage 1.

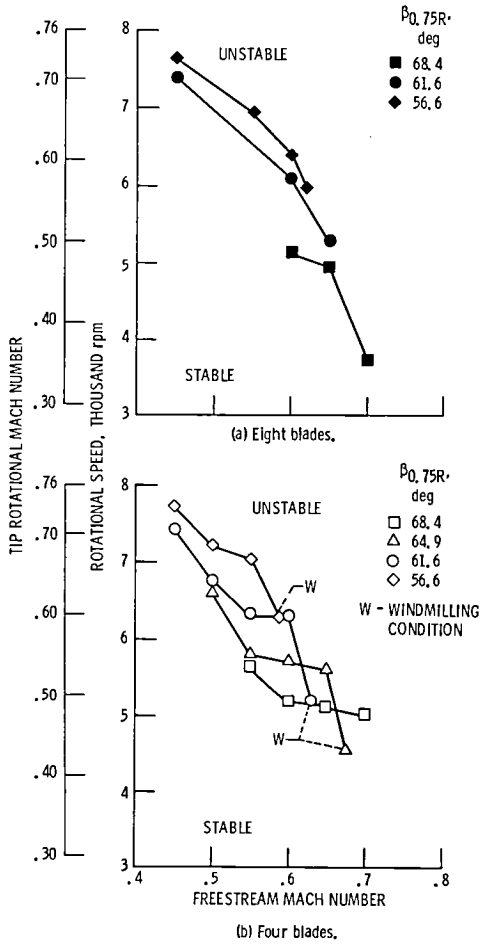

Figure 10. - Flutter conditions, SR3C-X2 model.

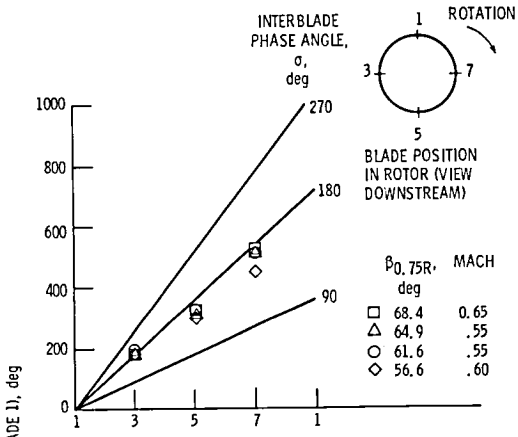

(a) Four-blade rotor.

(b) Eight-blade rotor.

Figure 11. - Blade phase angles at flutter.

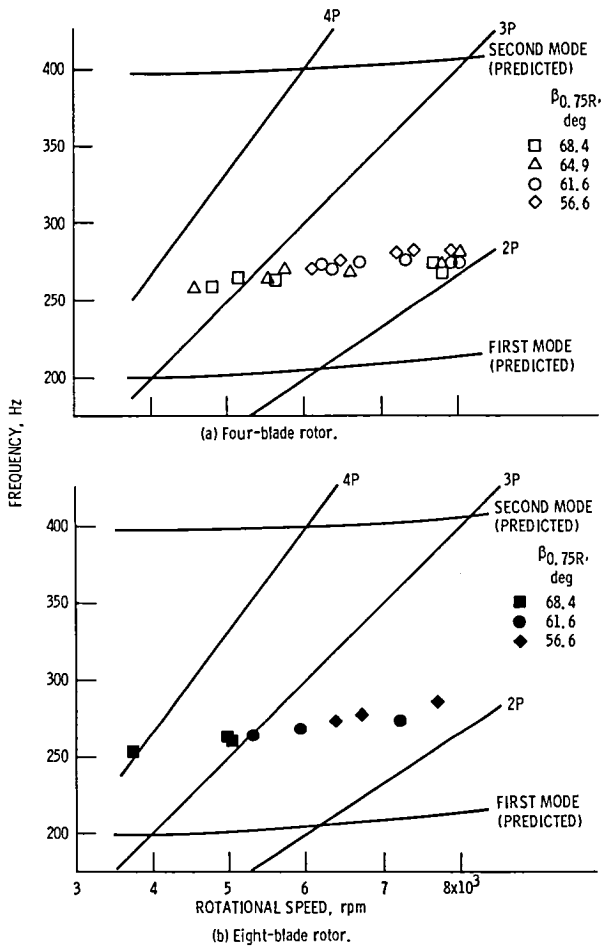

(a) Four-blade rotor.

(b) Eight-blade rotor.

Figure 12. - Measured flutter frequencies, SR3C-X2 model.

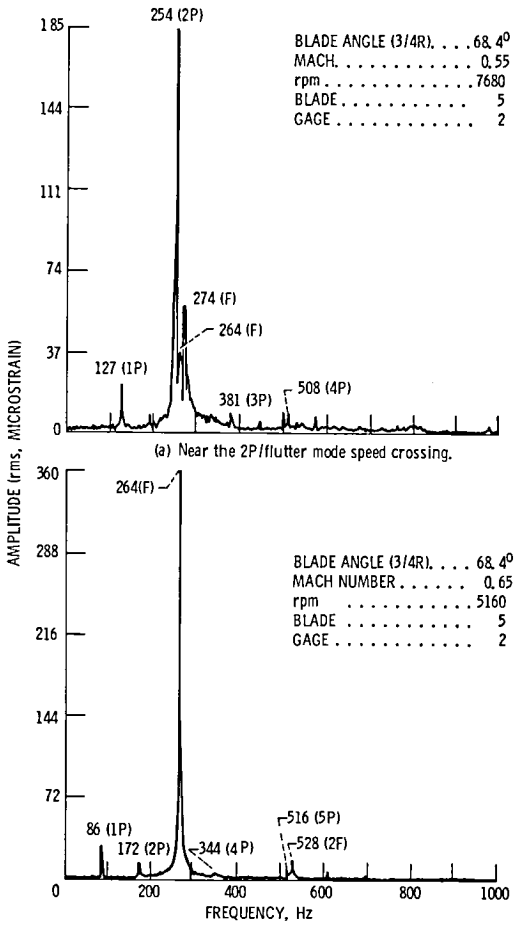

(a) Near the 2P/flutter mode speed crossing.

(b) Away from the 2P/flutter mode speed crossing.

Figure 13. - Strain amplitude spectrum, 4-blade rotor, SR3C-X model.

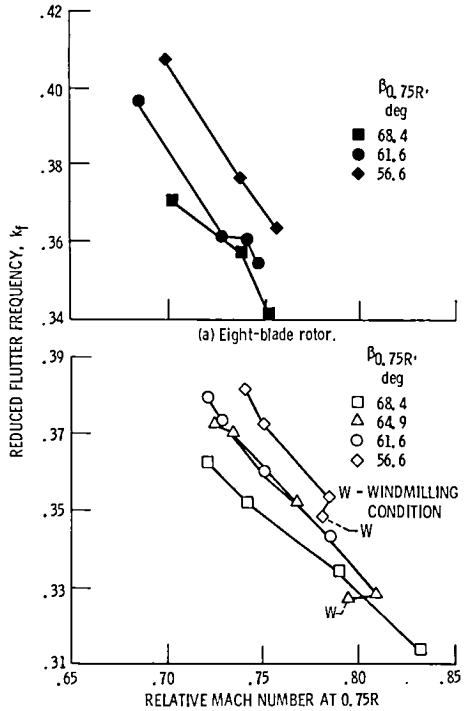

(b) Four-blade rotor.

Figure 14. - Flutter reduced frequency, SR3C-X2 model.

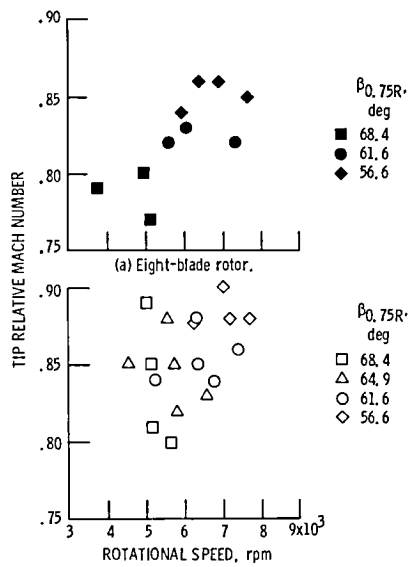

(b) Four-blade rotor.

Figure 15. - Tip relative Mach number at flutter, SR3C-X2 model.

1. Report No.	2. Government Accession No.	3. Recipient's Catalog No.
NASA TM-88792		

4. Title and Subtitle	5. Report Date
Experimental Classical Flutter Results of a Composite Advanced Turboprop Model	July 1986
	6. Performing Organization Code 535-03-12
7. Author(s)	8. Performing Organization Report No.
O. Mehmed and K.R.V. Kaza	E-3127
	10. Work Unit No.
9. Performing Organization Name and Address	11. Contract or Grant No.
National Aeronautics and Space Administration Lewis Research Center Cleveland, Ohio 44135	13. Type of Report and Period Covered Technical Memorandum
12. Sponsoring Agency Name and Address	14. Sponsoring Agency Code
National Aeronautics and Space Administration Washington, D.C. 20546	

15. Supplementary Notes

Material presented at the Bisplinghoff Memorial Symposium on Recent Trends in Aeroelasticity, Structures, and Structural Dynamics sponsored by the University of Florida, Gainesville, Florida, February 6-7, 1986.

16. Abstract

Experimental results are presented that show the effects of blade pitch angle and number of blades on classical flutter of a composite advanced turboprop (propfan) model. An increase in the number of blades on the rotor or the blade pitch angle is destablizing which shows an aerodynamic coupling or cascade effect between blades. The flutter came in suddenly and all blades vibrated at the same frequency but at different amplitudes and with a common predominant phase angle between consecutive blades. This further indicates aerodynamic coupling between blades. The flutter frequency was between the first two blade normal modes, signifying an aerodynamic coupling between the normal modes. Flutter was observed at all blade pitch angles from small to large angles-of-attack of the blades. A strong blade response occurred, for four blades at the two-per-revolution (2P) frequency, when the rotor speed was near the crossing of the flutter mode frequency and the 2P order line. This is because the damping is low near the flutter condition and the interblade phase angle of the flutter mode and the 2P response are the same.

17. Key Words (Suggested by Author(s))	18. Distribution Statement
Flutter; Advanced turboprop; Propeller; Propfan; Aeroelasticity	Unclassified - unlimited STAR Category 39

19. Security Classif. (of this report)	20. Security Classif. (of this page)	21. No. of pages	22. Price*
Unclassified	Unclassified		

*For sale by the National Technical Information Service, Springfield, Virginia 22161

National Aeronautics and
Space Administration

Lewis Research Center
Cleveland, Ohio 44135

NASA